Article ID: 1006-8775(2024)02-0168-12

Comparative Analysis of Energy Characteristics of Two Southwest Vortices in Sichuan Under Similar Circulation Backgrounds

ZHOU Chun-hua (周春花)[1], ZHANG Ju (张 驹)[2], XIAO Hong-ru (肖红茹)[3]

(1. Sichuan Meteorological Disaster Prevention Technology Center, Chengdu 610072 China; 2. Chengdu Meteorological Bureau, Chengdu 610072 China; 3. Sichuan Meteorological Observatory, Chengdu 610072 China)

Abstract: Based on ERA5 reanalysis data, the present study analyzed the thermal energy development mechanism and kinetic energy conversion characteristics of two extreme rainstorm processes in relation to the shallow southwest vortex in the warm-sector during a "rain-generated vortex" process and the deep southwest vortex in a "vortex-generated rain" process. The findings were as follows: (1) During the extreme rainstorm on August 11, 2020 (hereinafter referred to as the "8·11" process), intense surface heating and a high-energy unstable environment were observed. The mesoscale convergence system triggered convection to produce heavy rainfall, and the release of latent condensation heat generated by the rainfall promoted the formation of a southwest vortex. The significant increase (decrease) in atmospheric diabatic heating and kinetic energy preceded the increase (decrease) in vorticity. By contrast, the extreme rainstorm on August 16, 2020 (hereinafter referred to as the "8·16" process) involved the generation of southwest vortex in a low-energy and high-humidity environment. The dynamic uplift of the southwest vortex triggered rainfall, and the release of condensation latent heat from rainfall further strengthened the development of the southwest vortex. The significant increase (decrease) in atmospheric diabatic heating and kinetic energy exhibited a delayed progression compared to the increase (decrease) in vorticity. (2) The heating effect around the southwest vortex region was non-uniform, and the heating intensity varied in different stages. In the "8·11" process, the heating effect was the strongest in the initial stage, but weakened during the vortex's development. On the contrary, the heating effect was initially weak in the "8·16" process, and intensified during the development stage. (3) The available potential energy of the "8·11" process significantly increased in kinetic energy converted from rotational and divergent winds through baroclinic action, and the divergent wind energy continued to convert into rotational wind energy. By contrast, the "8·16" process involved the conversion of rotational wind energy into divergent wind energy, which in turn converted kinetic energy back into available potential energy, thereby impeding the further development and maintenance of the southwest vortex.

Key words: southwest vortex; similar circulation background; diabatic heating; kinetic energy; spatial non-uniform heating effect

CLC number: P458 **Document code:** A

Citation: ZHOU Chun-hua, ZHANG Ju, XIAO Hong-ru. Comparative Analysis of Energy Characteristics of Two Southwest Vortices in Sichuan Under Similar Circulation Backgrounds [J]. Journal of Tropical Meteorology, 2024, 30(2): 168–179, https://doi.org/10.3724/j.1006-8775.2024.015

1 INTRODUCTION

The southwest low vortex, also known as southwest vortex, is a closed, diminutive-scale atmospheric phenomenon characterized by cyclonic circulation at the 700 (or 850) hPa level in the western region of Sichuan. Its formation is intricately linked to the distinctive geographical setting and prevailing regional circulation patterns (Lu and Lei [1]; Xu [2]; Mao et al. [3]; Wang and Tan [4]; Feng et al. [5]; Zhu et al. [6]). Initially, the southwest vortex emerges as a shallow mesoscale system, with most instances dissipating or remaining confined to their source areas. However, under appropriate circulation conditions, a few vortices can extend beyond their origin and progress eastward. This eastward propagation is often accompanied by substantial precipitation events in the middle and lower reaches of the Yangtze River, the Huaihe River Basin, South China, and even North China (Fu et al. [7]; Zhang et al. [8]; Chen et al. [9]; Yu et al. [10]; Kuo et al. [11]; Fu et al. [12, 13]; Wang and Gao [14]). In terms of the intensity, frequency and scope of the rainstorms it causes, the southwest vortex ranks second only to typhoons and their residual low pressure systems (Wang et al. [15]). Statistics show that more than 52% of extreme rainstorms in the Sichuan Basin are induced by the southwest vortex (Zhou et al. [16]). Therefore, the study of the characteristics of the southwest vortex that induces extreme rainstorms is of great significance for the prediction of severe weather.

Because the generation and development of the

Received 2023-10-10; **Revised** 2024-02-15; **Accepted** 2024-05-15

Funding: Key Project of Joint Meteorological Fund of the National Natural Science Foundation of China (U2242202); Key Project of the National Natural Science Foundation of China (42030611); Innovative Development Special Project of China Meteorological Administration (CXFZ2023J016); Innovation Team Fund of Sichuan Provincial Meteorological Service (SCQXCX7D-202201)

Biography: ZHOU Chun-hua, primarily undertaking research on disaster weather forecast research.

Corresponding author: XIAO Hong-ru, e-mail:calf-dream@163.com

southwest vortex are mainly affected by the dynamic and thermodynamic processes associated with the plateau and the large-scale background, research on this topic mainly employs diagnostic analysis and numerical simulation as the main methods. Significant progress has been made in understanding the dynamic and thermodynamic characteristics of the southwest vortex through the application of vorticity budget, divergence, and apparent heat source equations. Existing studies have shown that the surface sensible heat significantly affects the generation of the southwest vortex (Chen and Li [17]; Hardy et al. [18]; Li et al. [19]; Cheng et al. [20]; Feng et al. [21]; Li et al. [22]; Ni et al. [23]; Chen [24]; Yang et al. [25]; Zhai et al. [26]), and the release of condensation latent heat by precipitation is conducive to the rapid development of the southwest vortex (Chen and Yang [27]; Chen and Li [28]). Diabatic heating determines not only the length of the life history of the southwest vortex but also the intensity of its development (Yu et al. [29]; Zhou et al. [30]). Numerical simulation experiments also indicate that surface heating plays a sustaining role in the development of the southwest vortex, and the development of the southwest vortex is mainly influenced by the heating effect of precipitation condensation latent heat, and the release of precipitation condensation latent heat largely determines the formation of the southwest vortex (Davis and Trier [31]; Ding et al. [32]; Qian and Zhao [33]). Li et al. [34] showed that before the generation of the warm vortex, the surface sensible heating and warm advection near the source area of the warm vortex contribute significantly to the generation of positive non-thermal wind vorticity. In a study of the kinetic energy of the southwest vortex, Ding et al. [35] stated that the upper tropospheric potential vortex disturbance significantly influences the development of the low vortex, and the high-value region of the upper potential vortex easily stimulates the formation of surface cyclones. Energy conversion within a low vortex and its external energy transport mainly occur during the changes of the potential energy and kinetic energy of the disturbance at mid-to-high levels, which can effectively reflect the changes in the intensity of the low vortex. Vertical energy transport also promotes the development of the low vortex system (Yang and Zhang [36]). The strengthening of low-level jets easily causes low-level convergence, promotes the rapid increase of mid-level potential vorticity, and reinforces the southwest vorticity into a deep system (Peng et al. [37]).

In mid-August 2020, extreme rainstorms occurred frequently in the western Sichuan Basin, and the rainfall in 10 days reached half of the annual rainfall, particularly from 20:00 on August 10 to 08:00 on August 11 (hereinafter referred to as the "8·11" process, BJT) and from 20:00 on August 15 to 08:00 on August 16 (hereinafter referred to as the "8·16" process). In the two extreme rainstorms in the western Sichuan Basin, the maximum rainfall intensity reached 156.8 and 118.4 mm respectively, and the maximum cumulative rainfall in 12 h reached 428.2 and 428.7 mm, respectively. The circulation patterns during these two events were similar, characterized by the generation and dissipation of the southwest vortex. The rapid development of the southwest vortex induced the generation of extreme rainstorms. The southwest vortex in the "8·11" process was shallow and only has a closed circulation at 850 and 700 hPa levels. This vortex appeared after the onset of rainfall, indicating a "rain-generated vortex" influenced by thermal effects (Li and Chen [38]). By contrast, in the process of "8.16", the southwest vortex developed deeply, extending up to 300 hPa at its peak. In this case, heavy rainfall was induced after the formation of the vortex, indicating "vortex-generated rain" influenced by dynamic effects. Why did the southwest vortices of different intensities produce extreme rainstorms under similar circulation backgrounds, and what were the differences in their occurrence and development mechanism? What were the differences in dynamic and thermal characteristics? All These issues need to be analyzed carefully. This study aims to examine the thermal forcing mechanism and kinetic energy conversion characteristics of shallow type and deep type southwest vortices to provide insights into the generation and development mechanisms of southwest vortices.

2 DATA AND METHODS

2.1 *Data*

In this study, we used four types of data: (1) ERA5 reanalysis data from the European Centre for Medium-Range Weather Forecasts (ECMWF), which have an hourly temporal resolution, a 0.25°×0.25° spatial resolution, and 37 vertical layers (https://cds.climate.copernicus.eu/). The dataset was utilized for weather analysis and investigating the dynamic and thermodynamic development mechanisms of the southwest vortex. (2) ERA5-LAND reanalysis data from the ECMWF, which have an hourly temporal resolution and a higher spatial resolution of 0.1°×0.1°. The dataset was used to analyze the surface sensible heat flux and latent heat flux distribution. (3) Hourly precipitation data observed by stations of the China Meteorological Administration. The dataset was used to assess the variations in rainfall associated with the southwest vortex. (4) MICAPS radiosonde data issued by the China Meteorological Administration. The dataset was used to analyze the environmental field.

2.2 *Thermal energy method*

The apparent heat source and water vapor sink are widely used in the diagnosis and analysis of the southwest vortex, plateau vortex, and plateau shear line. In this study, two equations were used to discuss the thermal development of the southwest vortex. The equations of apparent heat source and apparent water vapor sink in P coordinates are expressed as follows (Michio and Richard [39]):

$$Q_1 = C_p\left(\frac{\partial T}{\partial t} + V \cdot \nabla T + \left(\frac{P}{P_0}\right)^k \omega \frac{\partial \theta}{\partial p}\right) \tag{1}$$

$$Q_2 = -L(\frac{\partial q}{\partial t} + V \cdot \nabla q + \omega \frac{\partial q}{\partial p}) \quad (2)$$

where Q_1 is the apparent heat source, Q_2 is the apparent water vapor sink, and the three terms on the right are the local variations in temperature (vapor), the horizontal advection term of temperature (vapor), and the vertical transport terms of temperature (vapor), respectively. In Eqs. 1–2, C_p is the specific heat at a constant pressure, which is 1004.8416 J kg^{-1} k^{-1}, T is the temperature, and V is the horizontal wind vector. ω is the vertical wind velocity in the pressure coordinate, and θ is the potential temperature. k=0.2875, p_0=1000 hPa, q is the specific humidity, and L is the condensation latent heat, which is 2.5×10^6 J kg^{-1}.

The vertically integrated diabatic heating can be obtained using Eqs. 3–4:

$$< Q_1 >= \frac{1}{g}\int_{p_s}^{p_t} Q_1 \mathrm{d}p \quad (3)$$

$$< Q_2 >= \frac{1}{g}\int_{p_s}^{p_t} Q_2 \mathrm{d}p \quad (4)$$

where p_s is the surface pressure and p_t=100 hPa.

The complete-form vertical vorticity equation can be simplified by assuming that only the external heat source is retained for heating without considering friction dissipation or the development of tilt vorticity (Wu et al. [40]):

$$\frac{\partial \zeta}{\partial t} + V \cdot \nabla \zeta + \beta v = (1-k) \cdot (f+\zeta)\frac{\omega}{p} + (f+\zeta)\frac{Q}{\theta} + \frac{f+\zeta}{\theta_z}\frac{\partial Q}{\partial z} - \frac{1}{\theta_z}\frac{\partial v}{\partial x}\frac{\partial Q}{\partial x} + \frac{1}{\theta_z}\frac{\partial u}{\partial y}\frac{\partial Q}{\partial y} + R \quad (5)$$

The terms on the right side of Eq. 5 represent the effect of the ascending motion, heat source, spatially non-uniform diabatic heating, and residual error (R, which consists of the frictional dissipation, slantwise vorticity development, and computational error) on local variations in vorticity. p is the pressure, and θ is the potential temperature. $Q = Q_1 / C_p$ represents the diabatic heating rate in the thermodynamic equation, and Eq. 1 is used for calculation. Eq. 5 is used to explore the mechanism of the diabatic heating effect on vorticity.

2.3 *Kinetic energy method*

The original horizontal wind (V) is converted into rotational wind (V_R) and divergent wind (V_D) (Buechler and Fuelberg [41]):

$$V = V_R + V_D \quad (6)$$

The kinetic energy per unit mass is expressed as follows:

$$k = \frac{1}{2}V \cdot V = \frac{1}{2}V_R \cdot V_R + \frac{1}{2}V_D \cdot V_D + V_R \cdot V_D \quad (7)$$
$$= k_R + k_D + V_R \cdot V_D$$

The kinetic energy of an atmospheric volume in isobaric coordinates (A is the horizontal computational area) is as follows:

$$K = K_R + K_D + K_{RD} \quad (8)$$

where

$$K = \iint k, K_D = \iint k_D, K_R = \iint k_R, K_{RD} = \iint V_R V_D, \text{and} \iint = \frac{1}{gA}\iint \mathrm{d}x\mathrm{d}y\mathrm{d}p \quad (9)$$

In Eq. 9, K is the kinetic energy in a limited area (hereinafter referred to as kinetic energy), K_D is the divergent kinetic energy, K_R is the rotational kinetic energy, and K_{RD} is the kinetic energy of the interaction between the rotational and divergent winds. The sign of K_{RD} depends on the divergent and rotational wind directions.

The equation for rotational kinetic energy is expressed as follows (Buechler and Fuelberg [41]; Endlich [42]):

$$B\frac{\partial K_R}{\partial t} = \iint -V_R \cdot \frac{\partial V_D}{\partial t} + \iint -f(v_R u_D - u_R v_D) + \iint -\zeta(v_R u_D - u_R v_D) + \iint -\omega\frac{\partial k_R}{\partial P} + \iint -\omega V_R \cdot \frac{\partial V_D}{\partial P}$$
$$\mathrm{DK_R} \qquad I_R \qquad \mathrm{AF} \qquad \mathrm{AZ} \qquad B \qquad C$$
$$+ \iint -V_R \cdot \nabla\phi + \iint -\nabla \cdot kV_R + \iint V_R \cdot F$$
$$G_R \qquad \mathrm{HF_R} \qquad F_R \quad (10)$$

$$\frac{\partial K_R}{\partial t} = \iint -V_D \cdot \frac{\partial V_R}{\partial t} + \iint -f(v_R u_D - u_R v_D) + \iint -\zeta(v_R u_D - u_R v_D) + \iint -\omega\frac{\partial k_R}{\partial P} + \iint -\omega V_R \cdot \frac{\partial V_D}{\partial P}$$
$$\mathrm{DK_D} \qquad I_D \qquad \mathrm{AF} \qquad \mathrm{AZ} \qquad B \qquad C$$
$$+ \iint -V_D \cdot \nabla\phi + \iint -\nabla \cdot kV_D + \iint -\frac{\partial \omega k}{\partial P} + \iint V_D \cdot F$$
$$G_D \qquad \mathrm{HF_D} \qquad \mathrm{VF} \qquad F_D \quad (11)$$

where u_R and u_D are the zonal rotational and divergent wind components, respectively, v_R and v_D are the meridional rotational and divergent wind components, respectively, ω is the vertical velocity, f is the Coriolis parameter, φ is the geopotential, and F is the frictional force. The sum of AF, AZ, B, and C is hereinafter denoted

as $C(K_D, K_R)$, which is the conversion term between K_D and K_R, and $C(K_D, K_R)$ greater than 0 indicates the conversion from K_D to K_R. The term on the left-hand side, $DK_R(DK_D)$ is the change term of $K_R(K_D)$ and denotes the local change of $K_R(K_D)$. $I_R(I_D)$ is the change in $K_R(K_D)$ caused by the nonlinear interaction between rotational and divergent winds. AF is the geostrophic effect. Both AF and AZ are affected by the relative orientations and magnitudes of V_R and V_D. Term B describes the vertical exchange of K_R, while term C is related to the configuration of V_D with V_D and the vertical distribution of V_D. The term $G_R(G_D)$ is the generation term for $K_R(K_D)$, which indicates the conversion between $K_R(K_D)$ and the available potential energy owing to the cross-contour flow of $V_R(V_D)$. The term $HF_R(HF_D)$ denotes the horizontal flux divergence of K by $V_R(V_D)$. The term $F_R(F_D)$ represents friction and is related to the rotational (divergent) wind, denoting frictional processes and energy transfer between the resolvable and unresolvable scales of motion. VF is the vertical flux divergence term for K.

The dynamic energy budget of the rotational wind of the divergent wind in an open system is shown in Fig. 1, where A is the atmospheric available potential energy, DK is the local change in kinetic energy, and DK_{RD} is the local change in kinetic energy of the rotational wind interaction of the divergent wind.

3 COMPARISON OF THE SOUTHWEST VORTEX ACTIVITIES

3.1 *Comparison of the environmental characteristics*

The "8·11" and "8·16" processes had similar upper-level circulation backgrounds (figure omitted). The 500 hPa western Pacific subtropical high obstructed the eastward movement of the upper-air trough, resulting in its stagnation and subsequent impact on Sichuan. Under the background of the "Trough in the North and Vortex in the South", this scenario favored the development of the southwest vortex. The 200 hPa South Asian high in the upper troposphere was robust, with the Sichuan Basin situated on the eastern side of the high-pressure center. The divergence development of the upper layer promoted the convergence growth of the lower layer. However, environmental conditions were different. According to the radiosonde data from Wenjiang Station of the China Meteorological Administration (figure omitted), the "8·11" process exhibited a stratification pattern characterized by dryness at the top and wetness at the bottom. The temperature difference between 850 and 500 hPa reached 23°C, the K index was 42.8°C, the available potential energy of atmospheric convection amounted to 3292.8 J kg^{-1}, and the level of free convection was at 925 hPa, making it is easy to trigger the development of convection. In contrast, during the "8·16" process, the humidity throughout the layer was high, the available potential energy of convection was only 22.3 J kg^{-1}. The level of free convection was at 550 hPa, and the energy was low, necessitating significant lifting force to induce heavy rainfall.

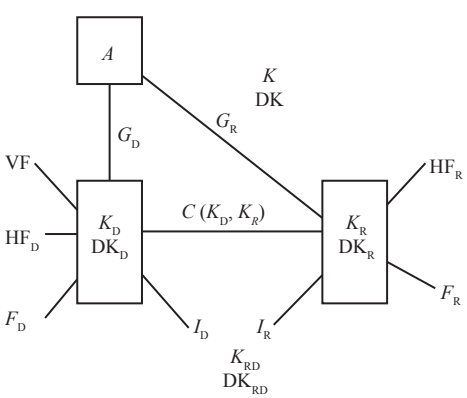

Figure 1. Schematic representation of the kinetic energy budget of divergent wind (rotating wind) in an open system.

3.2 *Activity path comparison*

From the hourly activity path of the southwest vortices (Fig. 2), the two processes were both active within the range of 28.5°–30.5°N and 102.8°–104.2°E. During the "8·11" process, the southwest vortex was generated and developed in Ya'an and traveled toward Yibin after 06:00 on August 11, weakening and disappearing. In contrast, the "8·16" process began in the west of Yibin, swiftly traveled northwest to Chengdu and rapidly developed, resulting in extreme precipitation in the western part of the basin.

During the "8·11" process, from 20:00 to 23:00 on August 10 (Fig. 3a), a mesoscale convergence system was formed in the southwest Sichuan Basin (Fig. 3a). There was a closed isobar of 141 dagpm in the height field, and convective cloud clusters developed in the center of the convergence system (figure omitted), triggering heavy local precipitation, and resulting in 26 stations of heavy rainfall above 50 mm h^{-1}. From 00:00 to 05:00 on August 11 (Fig. 3b), the circulation of the cyclone rapidly developed into a southwest vortex, and the height field was coordinated by a closed isobar of 140 dagpm. The

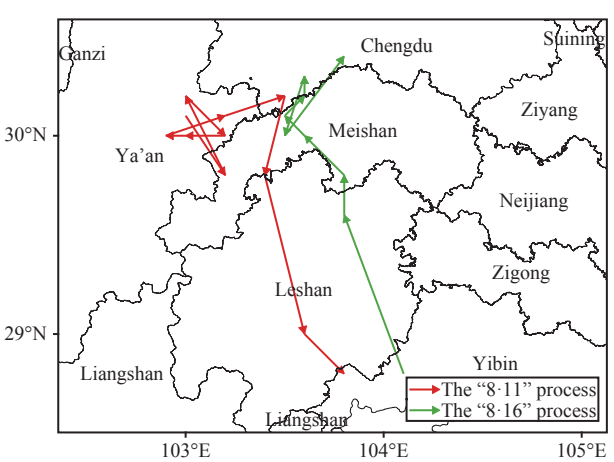

Figure 2. Hourly moving paths of the southwest vortices during the two processes in August 2020.

mesoscale convective cloud cluster further developed, the scale increased to 200 km (figure omitted), and the rainfall intensity peaked, with the maximum rainfall reaching 156.8 mm h^{-1}, resulting in 88 stations of heavy rainfall above 50 mm h^{-1}. After 06:00 on August 11 (Fig. 3c), the southwest vortex developed from south to north, the structure of the southwest vortex in the wind field was asymmetrical, the convective cloud cluster lifted northward, located over the northern part of the southwest vortex (figure omitted), and the rainfall intensity weakened. During the "8·16" process, from 20:00 to 23:00 on August 15 (Fig. 3d), the southwest vortex developed in the southwest of Sichuan Basin, with a closed isobar of 142 dagpm in the height field, and convective cloud cluster developed in the southwest vortex area (figure omitted), resulting in 5 stations of heavy rainfall above 50 mm h^{-1}. From 00:00 to 06:00 on August 16, the southwest vortex strengthened, with a closed isobar of 140 dagpm in the height field the circulation range increased. The convective cloud cluster increased to 250 km (figure omitted), resulting in 78 stations of heavy rainfall above 50 mm h^{-1}, and the maximum rainfall reached 118.4 mm h^{-1}. After 07:00 on August 16, the circulation weakened (Fig. 3f), as did the intensity and extent of the rainfall.

In summary, under the favorable circulation backgrounds of the "Trough in the North and Vortex in the South", the southwest vortex developed in both processes. The process of "8·11" constituted three stages: mesoscale disturbance, the rapid generation and development of the southwest vortex, and weakening. In a high-energy unstable environment, the mesoscale convergence system triggered the generation of heavy rainfall, and the release of condensation latent heat from the heavy rainfall promoted the generation and development of the southwest vortex, which was a typical process of the "rain-generated vortex." Meanwhile, the southwest vortex during this process was relatively shallow (Fig. 4), and the cyclonic circulation height only developed to 700 hPa. The resulting rainfall was localized and strong. The process of "8·16" constituted three stages: generation and the rapid development and weakening of the southwest vortex, heavy rainfall was triggered, and the release of condensation latent heat from the heavy rainfall strengthened the southwest vortex, which was a typical process of "vortex-generated rain." The southwest vortex developed extensively, and the cyclonic circulation height reached 300 hPa (Fig. 4). Heavy rainfall was widespread but slightly weak. In this section, the conversion characteristics of kinetic energy and the development mechanism of thermal energy in the two processes were analyzed.

4 COMPARISON OF THE THERMAL ENERGY CHARACTERISTICS OF THE SOUTHWEST VORTEX

4.1 *Surface diabatic heating*

A study conducted by Zhang and Wang [16] demonstrated that although the southwest vortex can be simulated without the surface heat flux, its intensity and position deviated significantly from the actual scenario, and the simulation results failed to replicate the precipitation patterns. Therefore, surface heating played a pivotal role in the development of the southwest vortex. This notion was supported by Li et al. [17], who asserted that prior to the

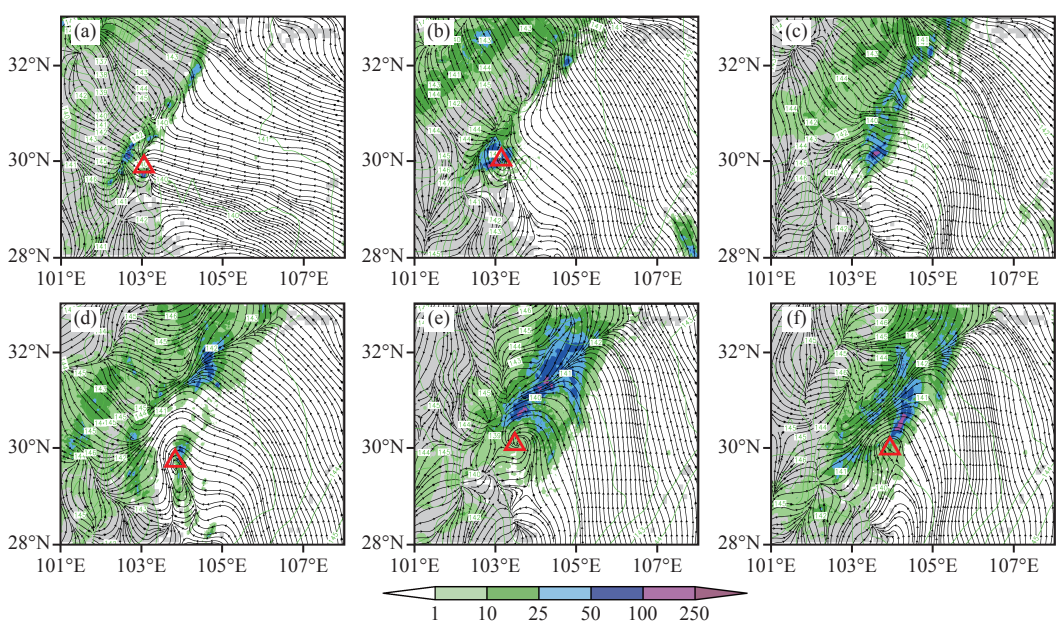

Figure 3. Flow field (850 hPa) and future three-hour rainfall for the two processes in August 2020 (colored, units: mm). The gray shadow is 850 hPa Tibetan Plateau topography, and the red triangle represents the geometric center of the southwest vortex. (a) At 20:00 on August 10; (b) at 02:00 on August 11; (c) at 06:00 on August 11; (d) at 21:00 on August 15; (e) at 03:00 on August 16; (f) at 7:00 on August 16.

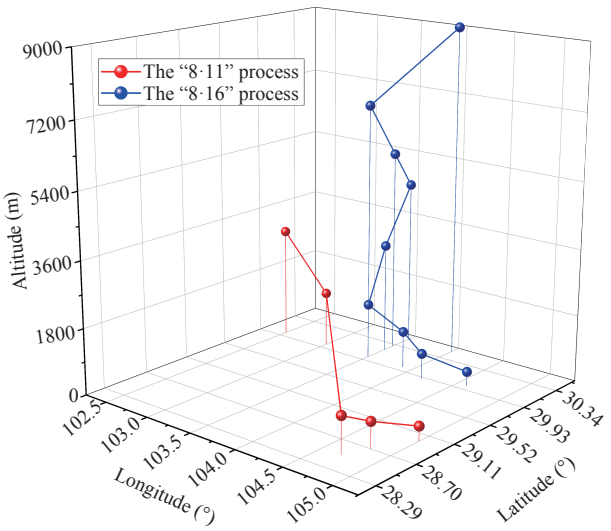

Figure 4. Variation in the southwest vortex center with height during the two processes in August 2020 at 02:00 on August 11, and at 03:00 on August 16.

formation of a warm vortex, surface sensible heating and warm advection in the vicinity of the vortex source contributed significantly to the generation of positive nonthermal wind vorticity, thereby underscoring the significance of surface heat flux. Fig. 5 illustrates the distribution of the average sensible and latent heat fluxes on the surface preceding the two rainfall processes. Throughout these processes, the latent heat flux surpassed the sensible heat flux. During the "8·11" process, there was a strong sensible heat flux in the southwest vortex generation region, and the sensible heat flux obtained by the atmosphere from the ground reached approximately 5×10^6–6×10^6 J m^{-2}, while the latent heat flux obtained by the atmosphere from the ground through turbulent diffusion also reached approximately 10×10^6–11×10^6 J m^{-2}. Strong ground heating caused the convergence system to generate and develop in the warm region. In the southwest vortex region of the "8·16" process, the surface sensible heat flux value was small, and there was nearly no heat exchange between the atmosphere and the surface.

4.2 *Atmospheric diabatic heating*

The relationship between diabatic heating, vorticity, and rainfall during the southwest vortex in the two processes was further analyzed, as depicted in the temporal variation diagram of the area average (Fig. 6, where the range of the area average was defined by the geometric center of the 850 hPa wind field of the southwest vortex [convergence system] serving as the center of the circle, and one longitude and latitude as the radius). In the "8·11" process (Fig. 6a), the vorticity increased rapidly over time, peaked at 04:00 on August 11, and then decreased rapidly. The variation trends of rainfall and positive vorticity were consistent. Atmospheric diabatic heating peaked at 01:00 on August 11, and the rapid increase (decrease) in diabatic heating preceded the increase (decrease) in positive vorticity. The vorticity and diabatic heating intensity in the "8·16" process were significantly stronger than those in the "8·11" process (Fig. 6b), and the vorticity peaked at 00:00 on August 16 and then decreased rapidly. The rainfall peaked at 01:00 on August 16, and the diabatic heating peaked at 02:00 on August 16 and then decreased rapidly. Therefore, the rapid increase (decrease) of positive vorticity preceded the increase (decrease) of diabatic heating.

4.3 *Thermal development mechanism*

Diabatic heating is closely related to the generation and development of the southwest vortex. The influence mechanism of the diabatic heating effect on the vorticity can be discussed using Eq. 5. According to Yao et al. [43], the magnitude of the other heat source terms is 10^{-11} s^{-2}. The spatial non-uniform diabatic heating term is 10^{-9} s^{-2}, and the variation in vorticity is primarily affected by the spatial diabatic heating effect. Therefore, the impact mechanism of the spatially non-uniform heating effect on the southwest vortex was analyzed based on representative time periods of 20:00 on the same day and the maximum hourly rainfall.

During the "8·11" process, at 20:00 on August 10

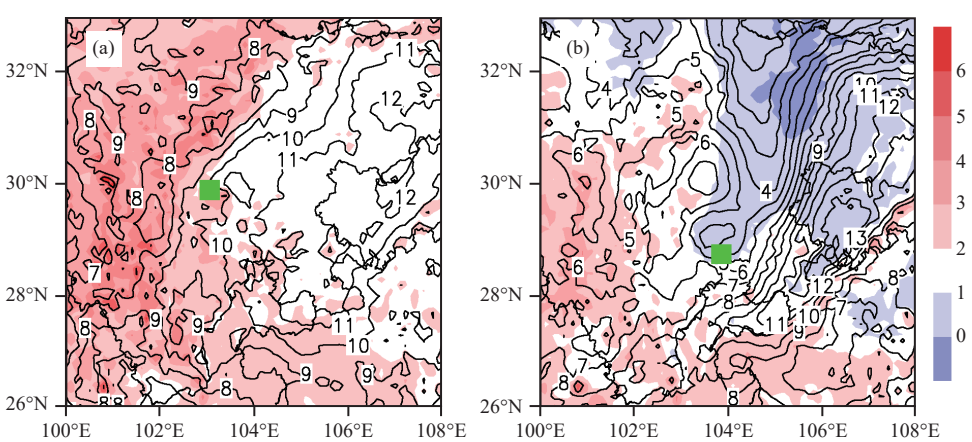

Figure 5. Average surface sensible heat flux (colored, units: 10^6 J m^{-2}, positive values upward) and latent heat flux (contour line, units: 10^6 J m^{-2}, positive values upward) of the two processes in August 2020, the green boxes indicating the location of the southwest vortex (convergence system) on the verge of generation. (a) Average from 16:00 to 19:00 on August 10; (b) average from 16:00 to 19:00 on August 15.

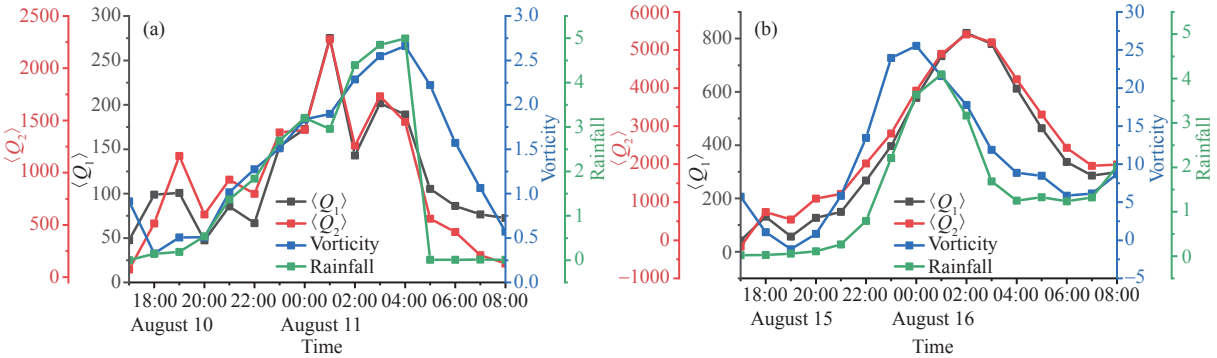

Figure 6. Vertical integral of diabatic heating (units: W m^{-2}), 850 hPa vorticity (units: 10^{-5} s^{-1}), and rainfall (units: mm) with time for the average area of the two processes in August 2020. (a) The "8·11" process; (b) the "8·16" process.

(Fig. 7a), the center of the convergence system tilted toward the southwest as the height increased, and the spatial non-uniform heating term was concentrated below 700 hPa, showing a heating effect around the southwest vortex and an asymmetric heating distribution on both sides of the southwest vortex. There was a 7×10^{-9} s^{-2} heating effect center on the northeast side of the southwest vortex. The heating effect promoted the generation of the southwest vortex and then strengthened the asymmetric development of the southwest vortex. At 02:00 on August 11 (Fig. 7b), the circulation center of the southwest vortex continued to tilt toward the southwest with the increase in height, and the non-uniform heating effect in the southwest vortex region weakened. The central value of the heating effect was only 2×10^{-9} s^{-2}, but the height increased to 600 hPa, which was also one of the reasons for the shallow southwest vortex.

During the "8·16" process, at 20:00 on August 15 (Fig. 7c), the center of the southwest vortex tilted westward as the height increased. The spatial non-uniform heating effect around the southwest vortex was mainly concentrated in the northeast of the southwest vortex, but the heating effect was weak, only 3×10^{-9} s^{-2}, and the heating height was only maintained below 700 hPa. At 03:00 on August 16 (Fig. 7d), the center of the southwest vortex developed vertically with the rise of height, and rose to 300 hPa, forming a deep southwest vortex, and the heating effect appeared around the

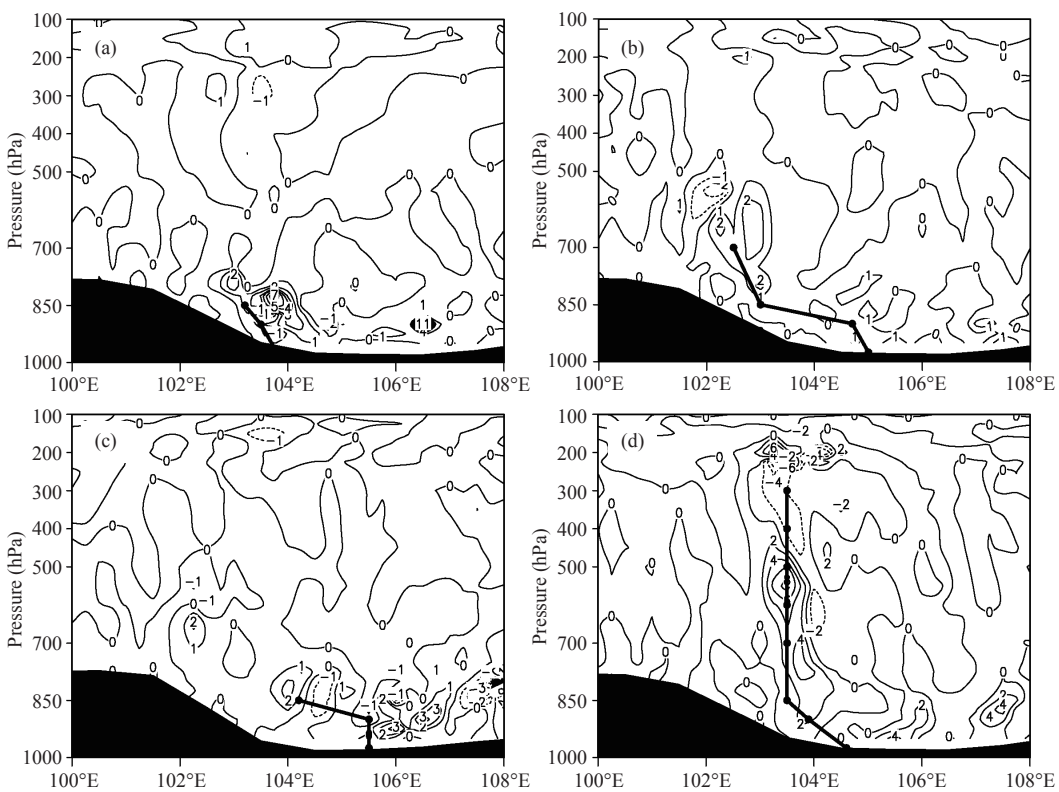

Figure 7. Vertical distribution of spatial non-uniform heating terms for the two processes in August 2020 (units: 10^{-9} s^{-2}). The black solid line is the geometric center of the southwest vortex circulation, and the black shadow is the terrain. (a) At 20:00 on August 10; (b) at 02:00 on August 11; (c) at 20:00 on August 15; (d) at 03:00 on August 16.

southwest vortex. The maximum value of the heating effect was nearly 500 hPa, and the extreme value reached 6×10^{-9} s^{-2}.

In summary, the non-uniform heating effect was present in the southwest vortex region, which was similar to findings obtained by Yao et al. [43]. In the process of "8·11", the heating effect was the strongest in the beginning stage, indicating that the thermal effect played a major role in the development of the southwest vortex in this process, while at the development stage of the southwest vortex it was weakened. Conversely, the heating effect of the "8·16" process was weak at the beginning stage, the heating effect was enhanced at the development stage, and the height of the non-uniform heating exceeded that of the "8·11" process.

5 KINETIC ENERGY CHARACTERISTIC COMPARISON

After comparing the temporal changes in average vorticity, K, K_R, K_D, and K_{RD} in the 850 hPa region and discussing the response of the kinetic energy and intensity evolution of the southwest vortex, we observed that the intensity of kinetic energy during the "8·16" process was significantly higher than that during the "8·11" process (Fig. 8). However, the trends of K, K_R, K_D, K_{RD}, and vorticity remained consistent. In the "8·11" process (Fig. 8a), kinetic energy reached its maximum at 01:00 and vorticity reached its maximum at 04:00. The increase (decrease) of kinetic energy was ahead of the increase (decrease) of vorticity. On the contrary, in the process of "8·16" (Fig. 8b), the vorticity reached its maximum at 00:00 and the kinetic energy reached its maximum at 03:00; the increasing (decreasing) trend of vorticity was ahead of the increasing (decreasing) of kinetic energy.

Table 1 presents the mean relative contributions of K, K_R, and K_{RD} to K_D in the southwest vortex region. In the two processes, K_R exhibited the most substantial contribution, which accounted for averages of 54.15% and 49.25%, respectively, followed by K_{RD}, which accounted for averages of 35.73% and 33%, and K_D represented the smallest proportion, which accounted for averages of 10.13% and 17.75%. During the "8·11" process, K peaked at 5.93×10^3 J m^{-2} at 20:00 on August 10. Simultaneously, the kinetic energy of K_{RD}, K_R, and K_D experienced an increase. At 02:00 on August 11, K decreased slightly, the kinetic energy of K_R increased significantly, and the proportion also increased to 67.8%. The increase in rotational wind energy promoted the development of the southwest vortex. At 08:00 on August 11, although K increased, K_R decreased, K_{RD} increased, and the divergence wind energy increased, which was not conducive to the development of the southwest vortex. During the "8·16" process, K increased significantly to 7.29×10^3 J m^{-2} at 20:00 on August 15, when the K_R intensity increased, the proportion decreased, and both the intensity and proportion of K_{RD} increased. At 02:00 on August 16, K further increased to 7.87×10^3 J m^{-2}, and the intensity and proportion of K_{RD} continued to increase, resulting in an increase in K_D kinetic energy and a decrease in K_R kinetic energy, which was not conducive to the continued strengthening of the southwest vortex. At the same time, the kinetic energy in the generation and rapid development stage of the southwest vortex in the "8.16" process was stronger than that in the "8·11" process, indicating that the south wind accompanied by the deep southwest vortex was stronger.

The conversion of kinetic energy between rotating and divergent winds led to changes in the dynamic energy of rotating winds, resulting in the generation and extinction of southwest vortex. The following paragraphs provide a detailed analysis of the kinetic energy conversion at each stage of the southwest vortex.

The "8·11" process was the pre-generation stage of the southwest vortex (Fig. 9a, and the transformation relationship of each physical quantity is shown in Fig. 1), The available potential energy A converted 0.019 and 0.008×10^3 J m^{-2} energy to the rotating wind K_R and the

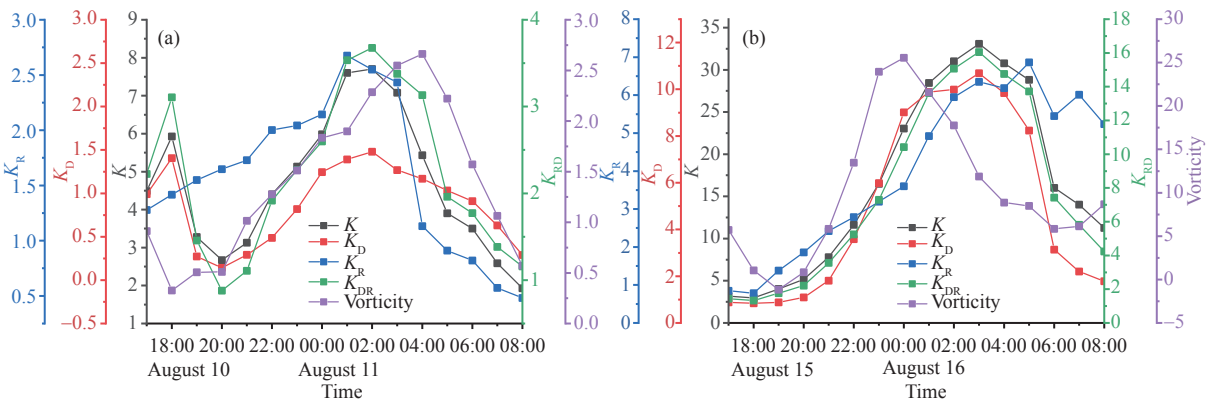

Figure 8. Evolution of K (black solid line, units: J m^{-2}), K_D (red solid line, units: J m^{-2}), K_R (blue solid line, units: J m^{-2}), K_{RD} (green solid line, units: J m^{-2}), and vorticity (purple solid line, units: 10^{-5} s^{-1}) over time within the southwest vortex range of 850 hPa in August 2020. (a) The "8.11" process; (b) the "8.16" process.

Table 1. Vertical integration of K, K_R, K_D, and K_{RD} from the surface to 500 hPa for the two processes in August 2020 (units: 10^3 J m^{-2}).

Time	K (%)	K_R (%)	K_D (%)	K_{RD} (%)
14:00 on August 10	4.47(100)	2.28(51)	0.48(10.7)	1.71(38.3)
20:00 on August 10	5.93(100)	2.98(50.3)	0.61(10.3)	2.34(39.4)
02:00 on August 11	4.78(100)	3.24(67.8)	0.22(4.5)	1.32(27.7)
08:00 on August 11	5.28(100)	2.51(47.5)	0.8(15)	1.97(37.5)
14:00 on August 15	3.99(100)	2.73(68.4)	0.33(8.3)	0.93(23.3)
20:00 on August 15	7.29(100)	4.24(58.2)	0.62(8.5)	2.43(33.3)
02:00 on August 16	7.87(100)	3.54(45)	1.46(18.6)	2.87(36.4)
08:00 on August 16	9.19(100)	2.33(25.4)	3.27(35.6)	3.59(39)

divergent wind K_D, respectively, through baroclinic and barotropic processes, increasing in the rotational wind and divergent wind energy. Then, the divergent wind energy converted 0.048×10^3 J m^{-2} energy to the rotating wind energy through the term $C(K_D,K_R)$. Therefore, the rotational wind energy increased and K increased, which was conducive to the generation of the southwest vortex. At the same time, in the friction and sub grid effects, the rotating wind V_R and the friction term F transported kinetic energy to the southwest vortex region, causing the HF_R and F_R values to reach 1.044 and 0.664×10^3 J m^{-2}, respectively, and I_R also transported 0.215×10^3 J m^{-2} energy to the southwest vortex. Moreover, increasing the rotational wind energy to 2.984×10^3 J m^{-2} was beneficial. Conversely, the kinetic energy was transported to the southwest vortex via divergence wind and friction, causing the HF_D and F_D values to reach 0.059 and 0.312×10^3 J m^{-2}, respectively. The above effects also caused the divergence wind energy to reach 0.61×10^3 J m^{-2}. In the rapid development stage of the southwest vortex (Fig. 9b), the overall trend was consistent with that of the pre-generation stage. The energy conversion of available potential energy A to K_R and K_D through baroclinic and barotropic processes increased significantly, 10 times that of the pre-generation stage, and the energy conversion to rotating wind and divergent wind dynamic energy reached 0.217 and 0.01×10^3 J m^{-2}, respectively. Although the energy converted from divergent wind dynamic energy to rotating wind dynamic energy decreased to 0.027×10^3 J m^{-2}, the kinetic energy transported by each component to the southwest vortex increased significantly, particularly, the HF_R, F_R, and I_R increased to 2.815, 0.74 and 0.729×10^3 J m^{-2}, respectively. HF_D and I_D also increased to 2.815 and 0.729×10^3 J m^{-2}, respectively. Under the joint action of each sub-term, $C(K_D,K_R)$ reached 0.027×10^3 J m^{-2}, causing the rotational wind energy to increase 3.24×10^3 J m^{-2}, thus promoting the development of the southwest vortex.

The "8·16" process was similar to the "8·11" process, but the available potential energy to kinetic energy conversion value was smaller. In the generation stage of the southwest vortex (Fig. 9c), the kinetic energy converted by the available potential energy A to K_R and K_D through baroclinic and barotropic processes was only 0.006 and 0.005×10^3 J m^{-2}. The rotating wind V_R and friction force work transported 2.62 and 0.652×10^3 J m^{-2} kinetic energy to the southwest vortex region, respectively, and the F_D term transported 0.309×10^3 J m^{-2} kinetic energy to the southwest vortex. However, owing to the negative effect of VF and HF_D terms on the southwest vortex, the divergent wind energy at this time was only 0.62×10^3 J m^{-2}. $C(K_D,K_R)$ reached 0.171×10^3 J m^{-2}, and the kinetic energy converted from divergent wind energy to rotating wind energy was 3–5 times that of the "8·11" process, causing K_R to reach 4.24×10^3 J m^{-2}, which was conducive to the generation and development of the southwest vortex. When the southwest vortex developed (Fig. 9d), the available potential energy A converted 0.027×10^3 J m^{-2} energy to the rotating wind energy. At the same time, HF_R had negative impact, and the I_R was only 0.269×10^3 J m^{-2}, which reduced the rotational wind energy. Furthermore, $C(K_D,K_R)$ was -0.135×10^3 J m^{-2}, and the rotational wind energy was converted to the divergence wind energy, causing a decrease in the rotational wind energy to 3.54×10^3 J m^{-2}. The divergent wind energy increased to 1.46×10^3 J m^{-2}, and finally, the divergent wind energy converted to the available potential energy A. The divergent wind V_D had negative impact, causing HF_D, I_R, and I_D to be constantly negative. The decrease in the rotational wind energy of the southwest vortex was not conducive to the maintenance and further development of the southwest vortex.

In summary, during the generation stage of the southwest vortex (pre-generation stage), the available potential energy was converted to divergent and rotational wind energy through barotropic and baroclinic processes. The divergent wind further converted the kinetic energy into rotational wind energy, thereby amplifying the rotational wind energy and fostering the generation and development of the southwest vortex. In the development stage, the energy converted from the available potential energy to the rotating wind energy in the "8·11" process was 10 times that in the "8·16" process, and the divergence wind energy was converted to the rotating wind energy, thereby promoting the development of the southwest vortex. However, during the "8.16"

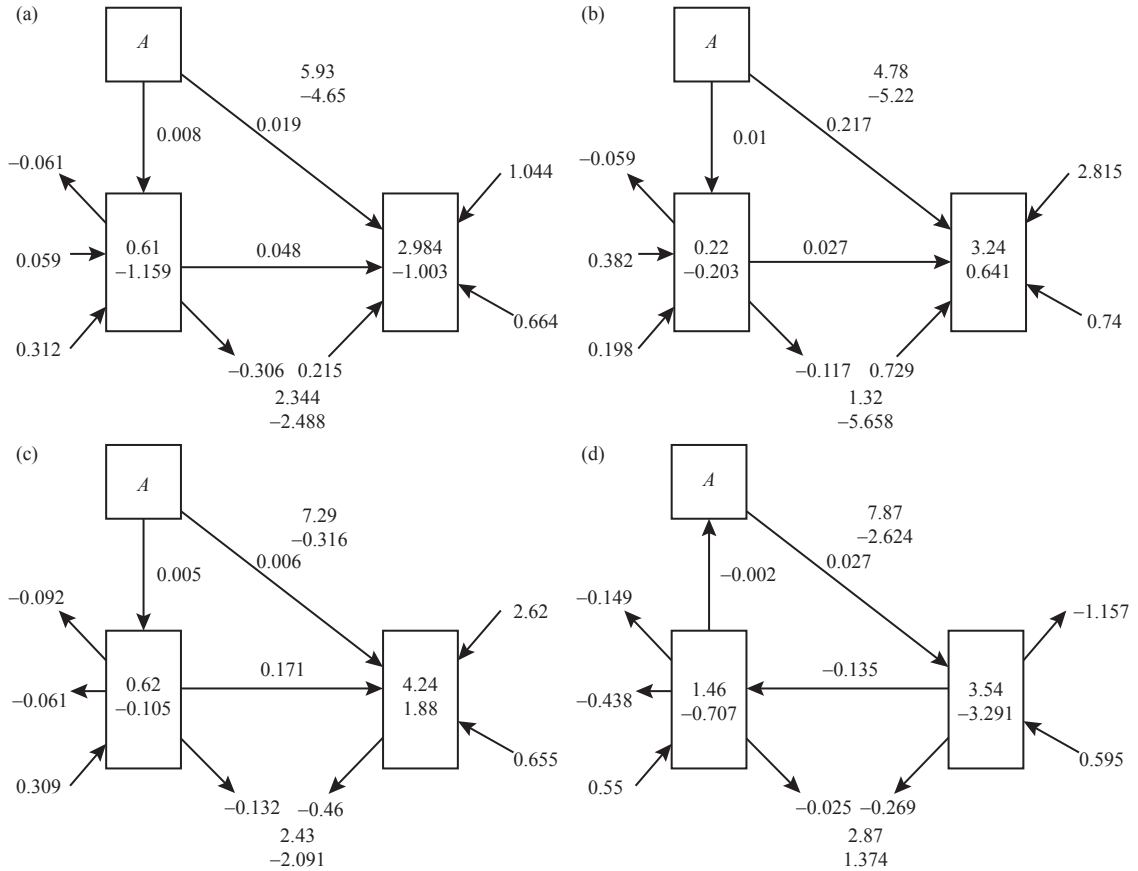

Figure 9. Dynamic energy budget of the southwest vortex divergence and rotational wind during the two processes in August 2020 (units: 10^3 J m^{-2}). (a) At 20:00 on August 10; (b) at 02:00 on August 11; (c) at 20:00 on August 15; (d) at 02:00 on August 16.

process, the conversion of rotational wind energy to divergent wind energy impeded the continued development and maintenance of the southwest vortex.

6 CONCLUSION AND DISCUSSION

Considering the two extreme rainstorm events associated with the southwest vortex in mid-August 2020, we utilized ERA5 reanalysis data to compare and analyze the thermal energy and kinetic energy characteristics of the shallow southwest vortices during a "rain-generated vortex" process in the warm sector and the deep southwest vortex during a "vortex-generated rain" process. Based on our analysis, the following conclusions were drawn.

The southwest vortex observed during the "8·11" process was generated in an environment characterized by strong surface heating and high energy. The mesoscale convergence system triggered convection, and the release of latent heat from condensation due to rainfall contributed to the formation and development of the southwest vortex. Conversely, during the "8·16" process, the southwest vortex formed in a low-energy environment. Dynamic uplift following the formation of the southwest vortex induced rainfall, and the release of latent heat from condensation promoted the further development of the vortex.

There was a significant correlation between atmospheric diabatic heating, kinetic energy, and changes in rainfall intensity. Sudden increases or decreases in diabatic heating and kinetic energy during the "8·11" process corresponded to changes in vorticity. Similarly, rapid changes in vorticity during the "8·16" process led to corresponding changes in diabatic heating and kinetic energy.

Non-uniform heating effect was present around the southwest vortex region, and the heating intensity varied in different stages. In the "8·11" process, the heating effect was the strongest in the initial stage, but weakened during the development stage. On the contrary, the heating effect was weak in the initial stage of the "8·16" process, and enhanced during the development stage.

Among the changes in kinetic energy, rotational wind energy exhibited the largest proportion, followed by divergent and rotational wind energies, with divergent wind energy being the smallest. During the generation or the pre-generation stages, the available potential energy was converted into divergent and rotational wind energies through barotropic and baroclinic processes. The divergent wind also converted kinetic energy into rotational wind energy, thereby augmenting the rotational wind energy and facilitating the formation and development of the southwest vortex. In the development stage, the available potential energy of the "8·11" process experienced a significant increase through the baroclinic effect, leading to an increase in the kinetic energy of the rotational and

divergent winds, which was ten-fold that of the "8·16" process. Moreover, divergent wind energy continued to be converted into rotational wind energy, thereby promoting the formation and development of the southwest vortex. Conversely, during the "8·16" process, rotational wind energy was converted into divergent wind energy, resulting in a reduction in rotational wind energy, which impeded the continue development and maintenance of the southwest vortex.

It is important to note that this study only compared and analyzed individual cases, and the findings cannot fully explain the characteristics of these weather processes. In the future, multiple dynamic synthesis analyses will be conducted for these weather scenarios to further understand the characteristics of southwestern vortices.

REFERENCES

[1] LU Jin-hua, LEI Xiao-tu. Preliminary analysis of movement of southwest vortex [J]. Journal of Chengdu Institute of Meteorology, 1996, 11(1): 40–49, in Chinese with English abstract

[2] XU Yu-hua. Southwest Climate [M]. Beijing: China Meteorological Press, 1991: 56–60, in Chinese.

[3] MAO Cheng-yan, QING Yi-yu, QIAN Zhi-tong, et al. Application of FY satellite data in precipitation of eastward-moving southwest China vortex: a case study of precipitation in Zhejiang Province [J]. Atmosphere, 2023, 14(11): 1664, https://doi.org/10.3390/atmos14111664

[4] WANG Qi-wei, TAN Zhe-min. Multi-scale topographic control of southwest vortex formation in Tibetan Plateau region in an idealized simulation [J]. Journal of Geophysical Research: Atmospheres, 2014, 119: 11543–11561, https://doi.org/10.1002/2014JD021898

[5] FENG Xin-yuan, LIU Chang-hai, FAN Guang-zhou, et al. Climatology and structures of southwest vortices in NCEP Climate Forecast System Reanalysis [J]. Journal of Climate, 2016, 29: 7675–7701, https://doi.org/10.1175/JCLI-D-15-0813.1

[6] ZHU Qian-gen, LIN Jin-rui, SHOU Shao-wen, et al. Principles and Methods of Meteorology (4th Edition) [M]. Beijing: China Meteorological Press, 2000, in Chinese.

[7] FU Shen-ming, LI Wan-li, SUN Jian-hua, et al. Universal evolution mechanisms and energy conversion characteristics of long-lived mesoscale vortices over the Sichuan Basin [J]. Atmospheric Science Letters, 2015, 16(2): 127–134, https://doi.org/10.1002/asl2.533

[8] ZHANG Yuan-chun, FU Shen-ming, SUN Jian-hua, et al. A 14-year statistics-based semi-idealized modeling study on the formation of a type of heavy rain-producing southwest vortex [J]. Atmospheric Science Letters, 2019, 20(5): e894, https://doi.org/10.1002/asl.894

[9] CHEN Yong-ren, LI Yue-qing, QI Dong-mei. Analysis of the convective characteristics during the mutual evolution of an inverted trough/low vortex and its induced rainstorm over the northeastern Sichuan Basin, China [J]. Meteorology and Atmospheric Physics, 2018, 131(4): 807–825, https://doi.org/10.1007/s00703-018-0607-4

[10] YU Zhuo-fu, MA Shuo, HAN Ding, et al. Physical and optical properties of clouds in the Southwest Vortex from FY-4A cloud retrievals [J]. Journal of Applied Meteorology and Climatology, 2022, 61(9): 1123–1138, https://doi.org/10.1175/JAMC-D-21-0128.1

[11] KUO Ying-hua, CHEN Lin-sheng, BAO Jian-wen. Numerical simulation of the 1981 Sichuan flood, Part Ⅰ: evolution of a mesoscale southwest vortex [J]. Monthly Weather Review, 1988, 116(12): 2481–2504, https://doi.org/10.1175/1520-0493(1988)116<2481:NSOTSF>2.0.CO;2

[12] FU Shen-ming, SUN Jian-hua, ZHAO Si-wei, et al. The energy budget of a southwest vortex with heavy rainfall over South China [J]. Advances in Atmospheric Sciences, 2011, 28(3): 709–724, https://doi.org/10.1007/s00376-010-0026-z

[13] FU Shen-ming, SUN Jian-hua, ZHAO Si-xiong, et al. An analysis of the eddy kinetic energy budget of a southwest vortex during heavy rainfall over South China [J]. Atmospheric and Oceanic Science Letters, 2009, 2(3): 135–141, https://doi.org/10.1080/16742834.2009.11446791

[14] WANG Zhi, GAO Kun. Sensitivity experiments of an eastward-moving southwest vortex to initial perturbations [J]. Advances in Atmospheric Sciences, 2003, 20(4): 638–649, https://doi.org/10.1007/BF02915507

[15] WANG Zuo-shu, WANG Yin-hui, LIANG Yi-guo. Numerical Study of a Southwest Vortex Heavy Rainfall Case [M]. Beijing: China Meteorological Press, 1996, in Chinese.

[16] ZHOU Chun-hua, XIAO Di-xiang, YU Shu-hua. Circulation background and structural characteristics of the southwest vortex inducing extreme rainstorm in Sichuan Basin [J]. Meteorological Monthly, 2022, 48(12): 1577–1589, https://doi.org/10.7519/j.issn.1000-0526.2022.081101, in Chinese with English abstract

[17] CHEN Yong-ren, LI Yue-qing. A thermodynamic condition affecting the movement of a southwest China vortex case [J]. Meteorology and Atmospheric Physics, 2022, 134: 36, https://doi.org/10.1007/s00703-022-00874-w

[18] HARDY S D, SCHULTZ M, VAUGHAN G. Early evolution of the 23–26 September 2012 UK floods: Tropical Storm Nadine and diabatic heating due to cloud microphysics [J]. Monthly Weather Review, 2017, 145(2): 543–563, https://doi.org/10.1175/MWR-D-16-0200.1

[19] LI Chao, LI Yan, FU Shen-ming, et al. A new perspective on the orographic effect of the windward slope on the multi-scale eastward-moving southwest vortex systems [J]. Atmospheric Research, 2022, 279: 106365, https://doi.org/10.1016/j.atmosres.2022.106365

[20] CHENG Xiao-long, LI Yue-qing, XU Li. An analysis of an extreme rainstorm caused by the interaction of the Tibetan Plateau vortex and the southwest China vortex from an intensive observation [J]. Meteorology and Atmospheric Physics, 2016, 128(3): 373–399, https://doi.org/10.1007/s00703-015-0420-2

[21] FENG Xin-yuan, LIU Chang-hai, FANG Guang-zhou, et al. Climatology and structures of southwest vortices in the NCEP climate forecast system reanalysis [J]. Journal of Climate, 2016, 29(21): 7675–7701, https://doi.org/10.1175/JCLI-D-15-0813.1

[22] LI Lun, ZHANG Ren-he, WEN Min. Diagnostic analysis of the evolution mechanism for a vortex over the Tibetan Plateau in June 2008 [J]. Advances in Atmospheric Sciences, 2011, 28(4): 797–808, https://doi.org/10.1007/s00376-010-0027-y

[23] NI Cheng-cheng, LI Guo-ping, XIONG Xiao-zhen. Analy-

sis of a vortex precipitation event over Southwest China using AIRS and in situ measurements [J]. Advances in Atmospheric Sciences, 2017, 34(4): 559–570, https://doi.org/10.1007/s00376-016-5262-4

[24] CHEN Yong-ren, LI Yue-qing, ZHAO Tian-liang. Cause analysis on eastward movement of Southwest China vortex and its induced heavy rainfall in South China [J]. Advances in Meteorology, 2015, 2015: 1–22, https://doi.org/10.1155/2015/481735

[25] PAN Yang, YU Ru-cong, LI Jian, et al. A case study on the role of water vapor from Southwest China in downstream heavy rainfall [J]. Advances in Atmospheric Sciences, 2008, 25: 563–576, https://doi.org/10.1007/s00376-008-0563-x

[26] ZHAI Dan-hua, KONG Fan-you, DAI Ze-jun, et al. Analysis of deep convective towers in a southwest-vortex rainstorm event [J]. Journal of Tropical Meteorology, 2021, 27(2): 177–190, https://doi.org/10.46267/j.1006-8775.2021.017

[27] CHEN Zhong-ming, YANG Kang-quan. A mechanism of the increment in convergence excited by the diabatic heating and the coupling forces between dynamic and thermodynamic fields [J]. Journal of Tropical Meteorology, 2010, 26(6): 711–715, in Chinese with English abstract

[28] CHEN Yong-ren, LI Yue-qing. Convective characteristics and formation conditions in an extreme rainstorm on the eastern edge of the Tibetan Plateau [J]. Atmosphere, 2021, 12(3): 381, https://doi.org/10.3390/atmos12030381

[29] YU Shi-wang, ZHANG Li-feng, WANG Yuan, et al. Mesoscale horizontal kinetic energy spectra of an eastward-moving Southwest vortex [J]. Atmosphere, 2022, 13 (5): 653, https://doi.org/10.3390/atmos13050653

[30] ZHOU Kuo, LIU Hai-wen, ZHAO Liang, et al. Binary mesovortex structure associated with southwest vortex [J]. Atmospheric Science Letters, 2017, 18(6): 246–252, https://doi.org/10.1002/asl.749

[31] DAVIS C A, TRIER S B. Mesoscale convective vortices observed during BAMEX, Part I: kinematic and thermodynamic structure [J]. Monthly Weather Review, 2007, 135: 2029–2049, https://doi.org/10.1175/MWR3398.1

[32] DING Wei-yu, WAN Qi-lin, HUANG Yan-yan, et al. MODIS brightness temperature data assimilation under cloudy conditions II: Impacts on rainstorm forecasting [J]. Journal of Tropical Meteorology, 2011, 17(3): 221–230, https://doi.org/10.3969/j.issn.1006-8775.2011.03.004

[33] QIAN Ting-ting, ZHAO Ping, ZHANG Fu-qing, et al. Rainy-season precipitation over the Sichuan Basin and adjacent regions in southwestern China [J]. Monthly Weather Review, 2015, 143: 383–394, https://doi.org/10.1175/MWR-D-1300158.1

[34] LI Guo-ping, WANG Jun, LU Jing-hua. A potential mechanism of the warm vortex genesis in Southwest China [J]. Journal of Applied Meteorological Science, 1991, 2(1): 91–99, in Chinese with English abstract

[35] DING Yi-hui. Diagnostic Analysis Methods in Weather Dynamics [M]. Beijing: Science Press, 1989, in Chinese.

[36] YANG Lian-mei, ZHANG Qing-yun. Energetic characteristics of a medium-range process of central Asian vortex [J]. Acta Meteorologica Sinica, 2014, 72(1): 182–190, https://doi.org/10.11676/qxxb2014.002, in Chinese with English abstract

[37] PENG Li-xia, SUN Zhao-bo, CHEN Hai-shan, et al. Analysis on the multi-center structure of summer South Asia high and its thermal influence factor [J]. Chinese Journal of Atmospheric Sciences, 2016, 40(5): 1089–1106, https://doi.org/10.3878/j.issn.1006-9895.1601.14310, in Chinese with English abstract

[38] LI Guo-ping, CHEN Jia. New progresses in the research of heavy rain vortices formed over the southwest China [J]. Torrential Rain and Disasters, 2018, 37(4): 293–302, https://doi.org/10.3969/j.issn.1004–9045.2018.04.001, in Chinese with English abstract

[39] MICHIO Y, RICHARD H J. Impacts of cumulus convection on thermodynamic fields [M]// EMANUEL K A, RAYMOND D J, eds. The Representation of Cumulus Convection in Numerical Models: meteorological monographs. Boston: American Meteorological Society, 1993: 39–40.

[40] WU Guo-xiong, LIU Huan-zhu. Complete form of vertical vorticity tendency equation and slantwise vorticity development [J]. Acta Meteorologica Sinica, 1999, 57(1): 1–15, https://doi.org/10.11676/qxxb1999.001, in Chinese with English abstract

[41] BUECHLER D E, FUELBERG H E. Budgets of divergent and rotational kinetic energy during two period of intense convection [J]. Monthly Weather Review, 1986, 114(1): 95–113, https://doi.org/10.1175/1520-0493(1986)114<0095:BODARK>2.0.CO;2

[42] ENDLICH R M. An iterative method for altering the kinematic properties of wind fields [J]. Journal of Applied Meteorology, 1967, 6(5): 837–844, https://doi.org/10.1175/1520-0450(1967)006<0837:AIMFAT>2.0.CO;2

[43] YAO Xiu-ping, LIU Qao-hua, ZHANG Shuo, et al. Mechanism of atmospheric diabatic heating effect on the intensity of zonal shear line over the Tibetan Plateau in boreal summer [J]. Journal of Geophysical Research: Atmospheres, 2021, 126: e2021JD034840, http://doi.org/10.1029/2021JD034840

Citation: ZHOU Chun-hua, ZHANG Ju, XIAO Hong-ru. Comparative Analysis of Energy Characteristics of Two Southwest Vortices in Sichuan Under Similar Circulation Backgrounds [J]. Journal of Tropical Meteorology, 2024, 30(2): 168–179, https://doi.org/10.3724/j.1006-8775.2024.015